Upper airway pressure distribution during nasal high-flow therapy

Hebbink, Rutger H J; Duiverman, Marieke L; Wijkstra, Peter J; Hagmeijer, Rob

Published in:
Medical Engineering & Physics

DOI:
10.1016/j.medengphy.2022.103805

Publication date:
2022

Medical Engineering and Physics 104 (2022) 103805

Contents lists available at ScienceDirect

Medical Engineering and Physics

journal homepage: www.elsevier.com/locate/medengphy

Upper airway pressure distribution during nasal high-flow therapy

Rutger H.J. Hebbink [*,a], Marieke L. Duiverman [b,c], Peter J. Wijkstra [b,c], Rob Hagmeijer [a]

[a] Engineering Fluid Dynamics, University of Twente, PO Box 217, Enschede 7500 AE, the Netherlands
[b] Department of Pulmonary Diseases/Home Mechanical Ventilation, University of Groningen, University Medical Center Groningen, the Netherlands
[c] Groningen Research Institute for Asthma and COPD, University of Groningen, the Netherlands

ARTICLE INFO

Keywords:
Nasal high-flow therapy
Pressure distribution
Positive end-expiratory pressure
Dead space washout
Upper airway

ABSTRACT

Two working mechanisms of Nasal High-Flow Therapy (NHFT) are washout of anatomical dead space and provision of positive end-expiratory pressure (PEEP). The extent of both mechanisms depends on the respiration aerodynamics and the corresponding pressure distribution: at end-expiration the onset of uniform pressure indicates the jet penetration length, and the level of the uniform pressure is the PEEP. The clinical problem is that adequate measurements in patients are presently impossible. In this study, the respiratory pressure distribution is therefore measured in 3D-printed anatomically correct upper-airway models of an adult and an infant. Assuming that elastic fluctuations in airway anatomy are sufficiently small, the aerodynamics in these rigid models will be very similar to the aerodynamics in patients. It appears that, at end-expiration, the jet penetrates into or slightly beyond the nasal cavity, hardly depending on cannula size or NHFT flow rate. PEEP is approximately proportional to the square of the flow rate: it can be doubled by increasing the flow rate by 40%. In the adult model, PEEP is accurately predicted by the dynamic pressure at the prong-exits, but in the infant model this method fails. During respiration, large pressure fluctuations occur when the cannula is relatively large compared to the nostrils.

1. Introduction

Nasal High-Flow Therapy (NHFT) is a method to provide non-invasive respiratory support to patients ranging from neonates to adults. A relatively high flow rate of heated, humidified and, optionally, oxygen-enriched air is supplied to the upper airway of a patient via a nasal cannula. The prongs of the nasal cannula are smaller than the nostrils, such that there is a loose fitting with an air leak. Via this leak, air can escape to the ambience at inspiration when the inspiratory flow rate is less than the device flow rate, or enter when the inspiratory flow rate exceeds the device flow rate. At expiration air escapes to the ambience. The working mechanisms of NHFT were first described by Dysart et al. [1], and in the present study the provision of Positive End-Expiratory Pressure (PEEP) and the washout of exhaled gases from the anatomical dead space are of interest.

There were initial concerns about the unpredictable level of PEEP generated by NHFT [2], which led to a number of studies in infants [3,4], adults [5], models of infants [6–9], and models of adults [10–13]. Although all studies report an increase in PEEP with increasing flow rate, the level of PEEP generated could not be described by the flow rate only. Opening of the mouth is widely reported to significantly reduce pressure [4–6,8,9], although one study found very little effect [3]. The infant's weight was found to be negatively correlated to pressure [3,4]. A larger outer diameter of the prongs, leading to higher occlusion rates, is associated with higher pressures [4,6,7,9,13], whereas a larger inner diameter of the prongs reduces PEEP [9]. Larger cannulae often have both larger inner (reducing PEEP) and outer (increasing PEEP) diameters. Consequently, the pressure in some adult models was hardly affected by cannula size [11], or decreasing with increasing cannula size [12].

The extent of both PEEP and washout depends on the respiration aerodynamics and the corresponding pressure distribution. When gravitational effects can be neglected, which is the case for air, fluid-mechanical principles dictate that pressure is uniform in any channel without flow. During respiratory pauses (e.g. at end-expiration), there is no nett-flow through the airways. The NHFT jet that enters the nostrils will therefore reverse at some point along the airway channel. Between that point and the alveoli, pressure must be (spatially) uniform and its value equals the PEEP. The onset of uniform pressure marks the penetration length of the jet, which is a measure for the washout effect of

* Corresponding author.
E-mail addresses: r.h.j.hebbink@utwente.nl (R.H.J. Hebbink), m.l.duiverman@umcg.nl (M.L. Duiverman), p.j.wijkstra@umcg.nl (P.J. Wijkstra), r.hagmeijer@utwente.nl (R. Hagmeijer).

https://doi.org/10.1016/j.medengphy.2022.103805
Received 20 December 2021; Received in revised form 14 April 2022; Accepted 14 April 2022
Available online 17 April 2022

NHFT. The further the jet penetrates into the nasal cavity, the higher the volume of CO_2-rich air that can be cleared. The level of uniform pressure during a respiratory pause equals PEEP. However, little data of the pressure distribution is currently available.

This paper presents measurements of the pressure distributions along infant and adult 3D-printed upper airway models, both without and with NHFT, and with or without respiration. The influence of cannula size, NHFT flow setting, and respiration on the pressure distribution is studied. The pressure distribution along the airway is used (a) to determine how the PEEP relates to cannula size and flow rate and (b) to estimate the jet penetration length into the upper airway.

2. Methods

2.1. Experimental setup

Rigid 3D-printed upper-airway geometries of an infant and an adult were used. The infant model is known as the SAINT-model [14], a Caucasian girl of 9 months. Since the model has a relatively small right nostril, a symmetric version was also constructed by mirroring the larger left nostril (including nasal cavity) over the nasal septum. This model will be referred to as "symmetric infant". Both models were printed using Digital Light Processing (DLP) with EnvisionTEC RC31 material. The male adult model was obtained from [15] and modified with permission from the author. It was printed using Selective Laser Sintering (SLS) with PA 12 nylon and, to prevent air leakage, impregnated afterwards. Both the infant and the adult models have closed mouths.

The digital models were modified to include small-diameter pressure-measurement holes normal to the airway walls. The locations, centred in the airway, are shown in Fig. 1a and b for respectively the asymmetric infant and the adult model, with labels indicated for later reference. The locations of the symmetric infant are identical to the left nasal cavity and the pharynx to trachea locations of the asymmetric infant. After 3D-printing, the holes were post-processed to ensure that the holes were open, and brass tubes were placed in (the outer part of) the holes. This appeared impossible in holes 1 and 2 in the asymmetric infant model, so these were closed. Hole 9L of the symmetric infant had to be closed because the brass tube broke off during construction. During the measurements, the pressure was measured at all locations using two pressure scanners (NetScanner model 9216, Measurement Specialities, Les Clayes-sous-Bois, France) with a sampling time of 6 ms (167 Hz).

To avoid condensation of water in the model and subsequent water build-up in the model and tubing, dry unheated air was supplied. By comparing the kinematic viscosity, it can be determined that heating to body temperature and fully humidifying the air typically decreases the Reynolds number with 8% compared to dry air at room temperature [16–18], which has hardly any effects on the flow field topology. Flow was obtained from a wall source, led through a flow controller (EL-FLOW Select F-201AV-50K-AAD-33-V, Bronkhorst, The Netherlands) and then into the inlet of the empty humidification chamber (MR290, Fisher & Paykel Healthcare Ltd., New Zealand) placed in the Airvo 2 system (Fisher & Paykel Healthcare Ltd., New Zealand). The Airvo device was turned off throughout the measurements, such that the use was restricted to making the connection between industrial fittings (flow controller) and medical connectors (the cannulae). Three different cannula sizes were used in both models. The inner and outer diameters of the cannulae and the occlusion rates in the nostrils of both models are summarized in Table 1. The nostril areas, used in the calculation of the occlusion rates, were estimated from the digital models. For more details about the cannulae and pictures of the cannulae in the noses of the adult and asymmetric infant, the reader is referred to a previous study [19]. It is noted that the calculated occlusion rate of the large cannula in the right nostril of the infant model exceeds 100%, meaning that the prong was somewhat compressed to fit into the nose. This is evidently clinically unacceptable, but the results are still included for reasons of completeness.

Table 1
Cannula dimensions and nostril occlusion rates.

	Cannula	d_{in} [mm]	d_{out} [mm]	Occlusion right nostril [%]	Occlusion left nostril [%]
Adult	S	4.8	5.4	13.7	13.3
	M	5.1 [13]	6.1 [13]	17.5	17.1
	L	6.0 [13]	7.2 [13]	24.4	23.8
Infant	S	1.35	3.0	79.4	50.5
	M	1.55 [20]	3.17 [20]	88.7	56.4
	L	2.35 [20]	3.82 [20]	129*	81.9
Symmetric infant	S	1.35	3.0	50.5	50.5
	M	1.55 [20]	3.17 [20]	56.4	56.4
	L	2.35 [20]	3.82 [20]	81.9	81.9

d_{in}: inner diameter of cannula; d_{out}: outer diameter of cannula; Outer diameter was determined at the widest point of the prong. Occlusion is defined as the total outer area of the prong divided by the estimated nostril area. *Calculated value; in practice occlusion equals 100% and the prong is slightly compressed.

A breathing simulator was connected to the trachea. Different respiratory patterns were obtained from literature and prescribed to the breathing simulator. Healthy [21] and COPD [22] respiratory profiles were tested for the adult model, and non-obstructed, moderately obstructed and severely obstructed patterns, all obtained from ref. [23], were tested for the infant models. The respiratory patterns were scaled to chosen tidal volumes and cycle lengths based on numbers representative for healthy subjects: 450 mL and 4 s for the adult and 85 mL and 1.76 s for the infants. More details about the breathing simulator and the respiratory profiles can be found in ref. [19].

2.2. Data collection and processing

For the measurements without respiration, pressures were recorded during 10 s for all settings (model, flow rate and cannula). The pressure at a certain location is calculated as the mean of all measured samples to limit the influence of sensor errors.

For the measurements with respiration, the respiratory profile was repeated continuously, causing constantly changing pressures in the 3D-printed model. Pressures were recorded during 50 s (infants) or 100 s (adult), resulting in approximately 25 full respiration cycles. Due to turbulence these cycles were not completely similar, also not after applying a low-pass filter, which complicates analysis. Therefore, a single representative pressure-time curve per measurement location was constructed from the recorded (unfiltered) signals as follows. The pressure-time signals were cut into N respiration cycles (approximately 25) based on the minima in the flow rate of the breathing simulator, and the times were shifted such that all cycles started at zero. Next, Fourier series with 20 frequencies, the same number as used for the prescribed respiratory curve, were constructed for all respiration cycles, such that N Fourier series were obtained. Lastly, a single pressure-time curve was constructed by taking the average of the N Fourier coefficients per frequency.

3. Results

The results are divided into two subsections. The first subsection presents the measurements without respiration (simulating a respiratory pause), the second presents the measurements with respiration. All pressures are relative to ambient conditions.

3.1. Without respiration

3.1.1. Pressure along the airway

The zero-respiration airway pressures are shown at various device flow rates for the adult model in Fig. 2a (small cannula) and Fig. 2b (large cannula), and for the infant model with small cannula in Fig. 3a (asymmetric nostrils) and Fig. 3b (symmetric nostrils). Results for the remaining cannula sizes are similar to the ones shown here and can be found as supplementary material. It is observed that the pressure in all cases becomes (approximately) uniform at some point, marking the penetration length of the jet. In front of this point (i.e. smaller distance from nostrils), two general trends are observed in the transition towards the uniform pressure: (a) the pressure increases towards the constant pressure (adult with small and medium cannula, left nostril of the infant model with all cannula sizes, and the symmetric infant model with all cannula sizes), or (b) the pressure decreases towards the constant pressure (adult with large cannula and right nostril of the infant model with all cannula sizes).

For the adult model, the pressure appears to be uniform from approximately 35 mm in the right nostril (pressure location 3R) or 55 mm in the left nostril (5L). The difference is most likely caused by anatomical differences. Despite the different pressure distributions with the different cannulae, there is no clear influence of the cannula size on the penetration length of the jet. Also the flow rate doesn't have a clear influence on the jet penetration length.

Similarly, the jet penetration length in the asymmetric infant model is influenced neither by the cannula size nor by the flow rate. The pressure is uniform from approximately 93 mm (location 20), just before the oropharynx starts (near location 21). Noteworthy, the jet extends further into the airway in the asymmetric infant model than in the adult model.

The symmetric infant model shows very different patterns compared to the asymmetric infant model. The pressure increases up to approximately 20 mm (location 3L and 3R) in both nostrils, beyond which it is almost constant over some distance. The pressure then converges at the end of the nasal cavity. Just like the other models, there is no clear influence of the cannula size or the flow rate on the pressure pattern. Although the right nostril is a mirrored version of the left nostril, the pressure appears to be slightly higher in the right nostril for all cases.

3.1.2. PEEP

The uniform pressures in the distal airway at zero-respiration conditions are, by definition, equal to the positive end-expiratory pressures (PEEP). The PEEP has been calculated for each case by taking the average of the three most distal data points. In Fig. 4 the PEEP in the adult model is plotted against the supplied flow rate for the different cannula sizes. It is observed that at a given flow rate the pressure is higher for smaller cannula sizes. The maximum PEEP generated is relatively low, approximately 300 Pa (about 3 cmH_2O) for 50 L/min flow and the small cannula. The figure also shows the dynamic pressure of the NFHT jet,

$$p_{dyn} = \frac{1}{2}\rho\left(\frac{Q_d}{2\frac{\pi}{4}d_{in}^2}\right)^2 = \frac{2\rho}{\pi^2 d_{in}^4}Q_d^2 \tag{1}$$

(ρ: air density in kg/m^3, Q_d: device flow rate in m^3/s, d_{in}: inner diameter of the cannula in m), and a power-law fit of the pressure to the device flow rate for each of the cannula sizes. It is seen that the dynamic pressure gives an accurate approximation of the delivered PEEP for all cannula sizes in the adult model. For frictionless steady flow, the PEEP would equal the sum of the static pressure and the dynamic pressure (Bernoulli's principle). Hence, PEEP is equal to the dynamic pressure when losses between the prongs and the trachea are small and the static pressure at the prongs is close to atmospheric pressure, which is expected for low nostril occlusion.

A similar plot for the asymmetric infant model is presented in Fig. 5a. It is observed that, in contrast to the adult model, pressure increases for larger cannulae, although the differences are, especially at lower flow rates, small. Since the dynamic pressure decreases for a larger cannula (at a given flow rate), it is clear that the PEEP cannot be approximated by the dynamic pressure in this case. Indeed, large differences between PEEP and dynamic pressure are observed for all cannula sizes. Clearly, the situation of frictionless steady flow with nearly atmospheric pressure at the prongs does not hold for this model. It is seen that the exponents of the power-law fits are lower than in the adult case, around 1.8. This may indicate a different flow behaviour compared to the adult model.

Finally, the PEEP for the symmetric infant is shown in Fig. 5b. The pressure increases with cannula size, but the difference between the small and medium cannula is small. It is observed that the pressure levels generated by the small and medium cannula are much lower compared to the asymmetric infant model. Clearly, a high occlusion rate in only one nostril already results in high levels of PEEP.

3.2. With respiration

3.2.1. Airway and cannula resistance

The resistance of the airway to respiratory flow has been investigated by measuring the pressures during respiration without a cannula. The results for the healthy (adult) and non-obstructed (infants) respiratory profiles are shown in Figs. 6, 7 a and b at several locations: the first available points in both nostrils, the first point behind the point where the two nasal cavities merge, a point near the beginning of the oropharynx, and the last point in the trachea. For the symmetric infant model, two additional points (3L and 3R) have been included to compare to the original geometry. It is observed that the pressure drop over the whole nasal cavity is higher for the symmetric infant model than for the asymmetric infant model. A more thorough investigation of all measurement locations shows that there is a relatively large pressure drop between points 8 and 7 in both nostrils in the symmetric infant, which is absent in the asymmetric infant. This indicates that there is a constriction in the symmetric infant at this point.

The airway resistance of the models, defined as the pressure drop from the trachea to the atmosphere divided by the respiratory flow rate, is shown in Table 2 for peak inspiration and peak expiration during the healthy (adult) or non-obstructed (infants) respiratory profile. It is noted that the airway resistance is flow-dependent, and hence the absolute values of the resistance change for the various respiratory profiles. Insertion of the cannula (without applying NHFT) increases the aerodynamic resistance. The percentile change in resistance due to the inserted cannula is shown in the table as well. For the adult model, the added resistance is low: less than 10% increase for all cases. In contrast, the resistance is increased significantly in both infant models. Where the increase may still be considered reasonable for the small and medium cannula in the symmetric infant model, increases of over 60% are observed during peak expiration for the large cannula. For the asymmetric infant model, which has a highly occluded right nostril, even the smallest cannula increases the resistance during expiration by almost 70%.

3.2.2. Airway pressures during NHFT

The pressure in time at the various locations with NHFT are shown in Fig. 8a and b for the adult model with the small and large cannula, respectively. Similarly, Fig. 9a and b show the pressure in respectively the asymmetric infant and symmetric infant model with small cannula. In all plots, the PEEP (determined as described in Section 3.1.2) is shown to indicate the inspiration (tracheal pressure below PEEP) and expiration (tracheal pressure above PEEP) phases. Also the results without NHFT are presented, showing the increased pressure due to the cannula.

The base level of the pressure and the pressure amplitude increases when flow is supplied through the cannula. Also the distribution of the pressure changes: the pressure drop during expiration over the nose

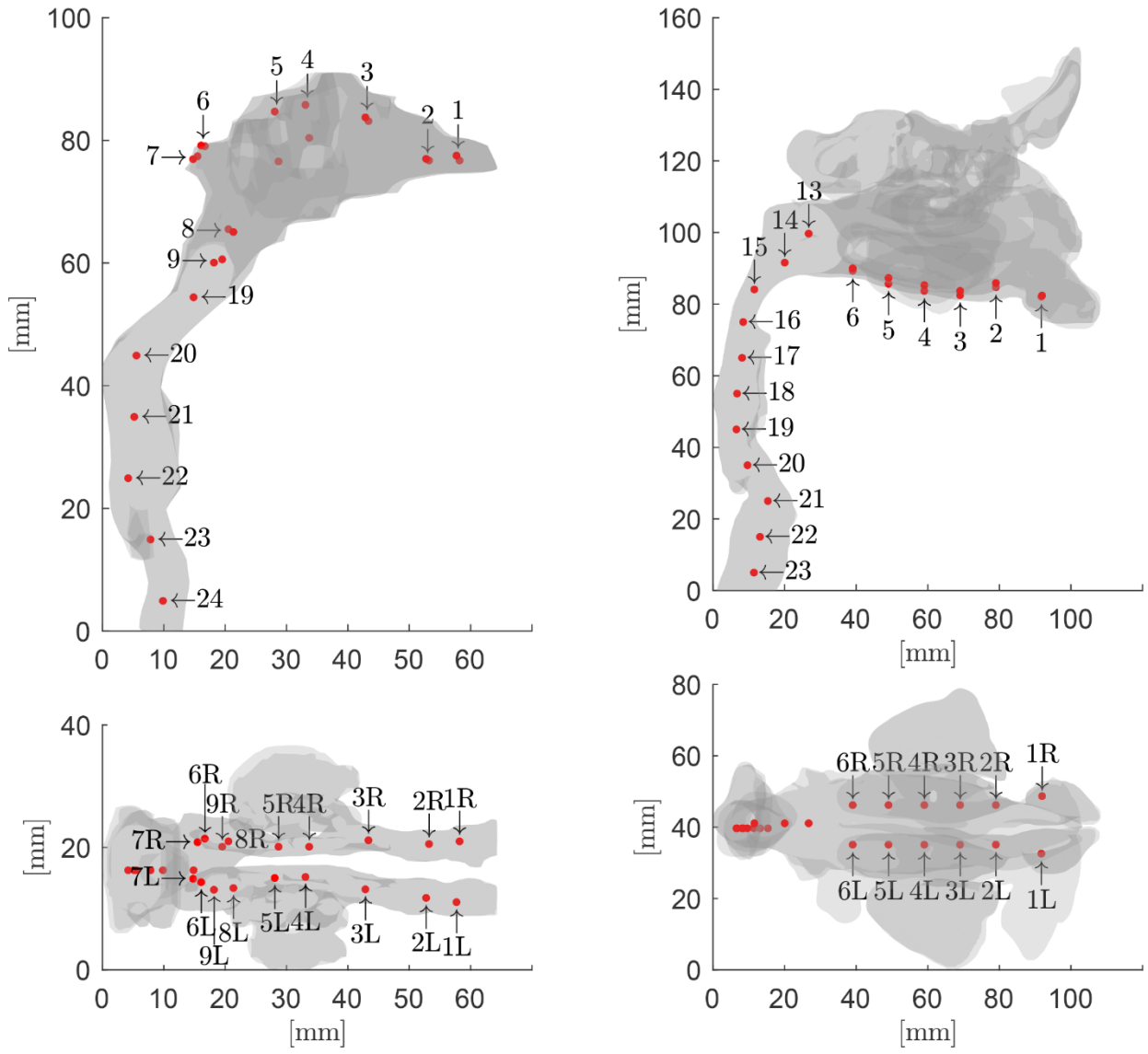

(a) Asymmetric infant (b) Adult

Fig. 1. Side (top panel) and bottom view (bottom panel) of the infant and adult airway with the pressure measurement holes indicated. The pressure measurement holes are labelled for later reference, where higher numbers are located deeper to the lungs, and L and R refer to left and right, respectively. The nostrils are located at the right-hand side, the trachea is at the bottom in the top panel.

(adult) or over the nasal cavity (infant) is increased compared to the pressure drop over the entire model. This is the result of the reversing jet, which increases the flows in the nose, but not in the trachea due to the limited jet-penetration length. Hence, the observed pressure distributions during expiration are comparable to those observed without respiration. When the device flow rate exceeds the inspiratory flow rate, there is also a nett outflow of air during inspiration. In the adult model, where all pressures are positive for the highest flow rate, similar pressure distributions are observed as for the case without respiration: pressures in the nose are lower than in the trachea for the small cannula, and higher for the large cannula. Lastly, it is important to note the effect of nostril occlusion in the asymmetric infant model. With high flow rates, the pressure in the narrow right nostril equals the pressure in the nasopharynx, or, for the fully occluding large cannula, even exceeds tracheal pressures.

4. Discussion

This study reveals the pressure distribution along upper airway geometries of an adult, asymmetric infant, and symmetric infant experimentally, with and without respiration and NHFT. From these measurements, PEEP was determined, the jet penetration length was estimated, the added airway resistance due to the cannula was determined, and the influence of NHFT on airway pressure was shown. Although PEEP and washout during NHFT have been a popular research topic during recent years, the present study is, to the authors' knowledge, the first one with measured pressures at a relatively fine spacing along the airway. The remainder of this section discusses the relations of the pressure distribution to PEEP and washout, and the limitations of the study.

4.1. PEEP

The observed PEEP in the adult model is relatively low, with a maximum of about 300 Pa (approximately 3 cmH_2O) at 50 L/min of NHFT. PEEP is considered to be one of the main working mechanisms of NHFT [1], and NHFT is sometimes used instead of Continuous Positive Airway Pressure (CPAP) because of the improved patient comfort [24].

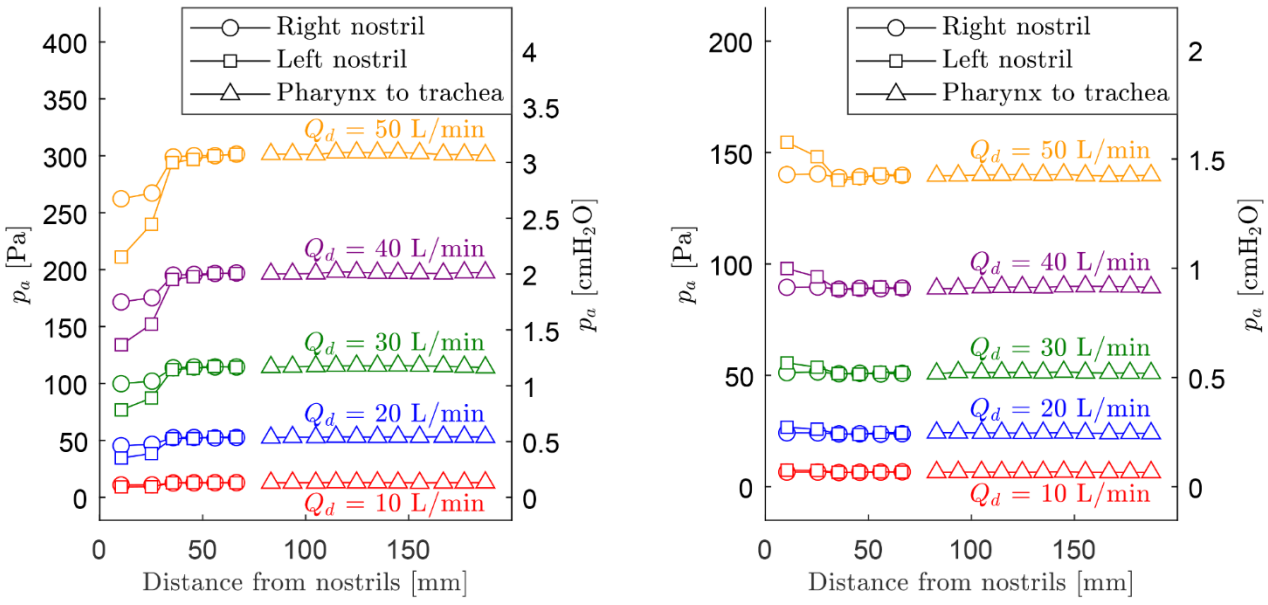

(a) Small cannula (b) Large cannula

Fig. 2. Adult model: pressure (p_a) along the airway without respiration for different device flow rates (Q_d) with two cannula sizes.

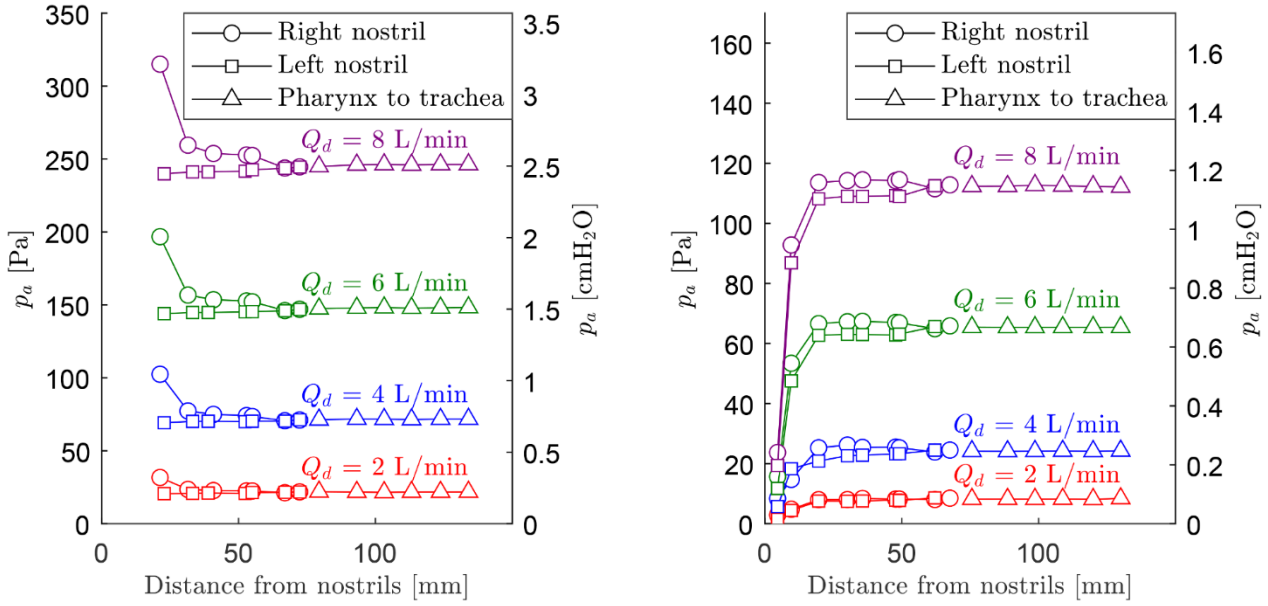

(a) Asymmetric infant model (b) Symmetric infant model

Fig. 3. Infant models: pressure (p_a) along the airway without respiration for different device flow rates (Q_d) using the small cannula.

However, the levels of PEEP measured in the adult model in this study are significantly lower than the PEEP provided in CPAP. Earlier studies on NHFT show both higher [5,12,13] and lower [11,13] levels of PEEP than found in this study, but comparison is difficult because of the use of different geometries. From a clinical point of view, the finding that PEEP is close to the dynamic jet pressure in the adult model may be relevant. Possibly, this might be a good way to approximate PEEP for low occlusion rates, but further verification is required.

In the asymmetric infant model, PEEP levels over 1000 Pa (approximately 10 cmH_2O) are observed with the large cannula. For the small and medium cannula with the maximum flow rate (8 L/min), PEEP is still relatively limited with less than 300 Pa (approximately 3 cmH_2O). In other studies, observed PEEP levels were either lower [9], or both lower and higher depending on the occlusion rate [7,20]. It is recommended by Kushida et al. [25] to start CPAP at minimally 4 cmH_2O (392 Pa) in patients with obstructive sleep apnea. These pressure levels are only observed in the present study when using the large (fully obstructive) cannula, or by exceeding the maximum prescribed flow rate with smaller cannulae. Hence, PEEP will most likely be below CPAP levels in clinical practice, unless highly occluding cannulae are used.

The symmetric infant clearly shows lower PEEP levels for the small and medium cannula than the asymmetric infant. Interestingly, PEEP in the symmetric infant with large cannula (81.9% occlusion) is very similar to PEEP in the asymmetric infant with small cannula (79.4% and 50.5% occlusion). Hence, it seems that PEEP is to a large extent determined by the most occluded nostril. From a clinical point of view, this implies that the smallest nostril should be leading in the selection of the cannula size. It is noted, however, that a single-prong cannula may

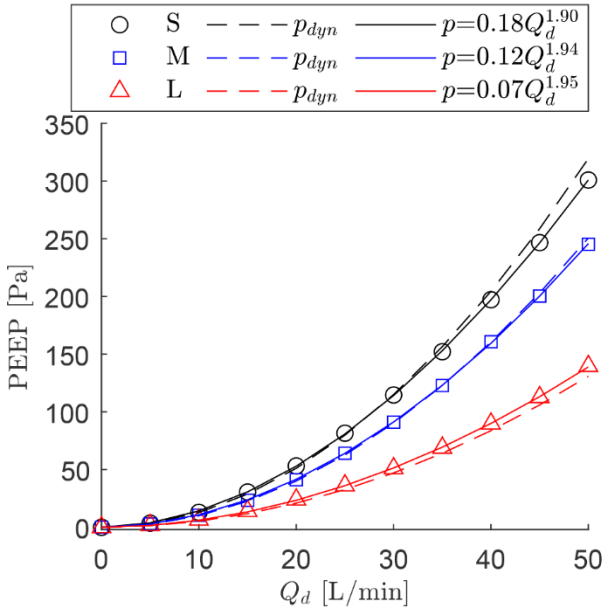

Fig. 4. Adult model: Positive End-Expiratory Pressure (PEEP) against device flow rates (Q_d) for three cannula sizes, compared with the dynamic pressure (p_{dyn}).

generate lower pressures than the equally-sized double-prong cannula [9], indicating that the occlusion of the other nostril cannot be neglected. More research on the single-prong cannula is desired, especially because of the unexpected lower pressure when the dynamic jet pressure is four times higher at the same flow rate.

The relation between cannula size and PEEP appears to be contradictory: whereas PEEP decreases with cannula size in the adult model, the reverse is true for the infant models. For the used cannulae, an increase in cannula size has two effects: the increase in outer diameter, leading to a higher nostril occlusion rate which increases PEEP, and a larger inner diameter, resulting in a lower dynamic pressure of the NHFT jet which reduces PEEP. In the adult model, occlusion rates were low: less than 25%. Indeed, the increase in airway resistance due to the cannulae appears to be very limited, and therefore it seems plausible that the increase of the inner diameter (reducing PEEP) has a more pronounced effect than the increase of the outer diameter (increasing PEEP). Consequently, the smallest cannula generates the highest PEEP. In contrast, the occlusion rates in the infant models are higher: at least 50%. Airway resistance indeed increases markedly by these cannulae, and consequently the effect of occlusion rate dominates over the lower jet pressure. It should be noted that the effect of PEEP with cannula size can also depend on the cannula geometry, which was different for the infant and the adult model. Presumably the highest PEEP can be delivered using a thick wall cannula with small inner and large outer diameter.

From a clinical point of view, it is important to note that all measurements in the present study indicate that the PEEP level behaves approximately quadratic in the flow rate. This roughly means that the PEEP is doubled when the flow rate is increased by 40%.

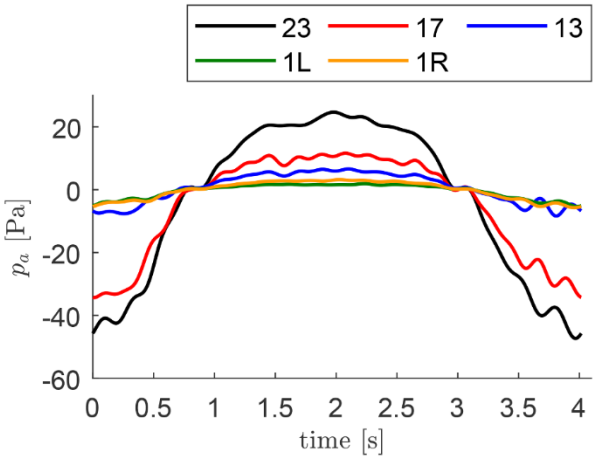

Fig. 6. Adult model: airway pressure (p_a) as a function of time at various locations (as indicated in Fig. 1b) during healthy respiration without a cannula.

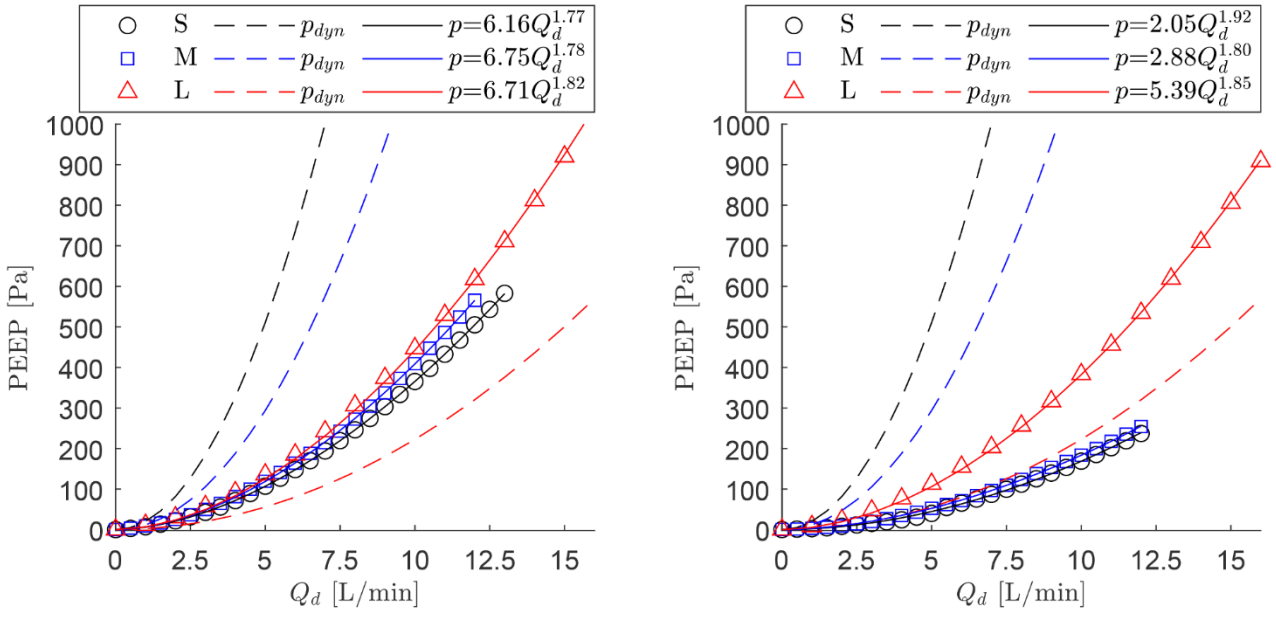

(a) Asymmetric infant model

(b) Symmetric infant model

Fig. 5. Infant models: Positive End-Expiratory Pressure (PEEP) against device flow rates (Q_d) for three cannula sizes, compared with the dynamic pressure (p_{dyn}).

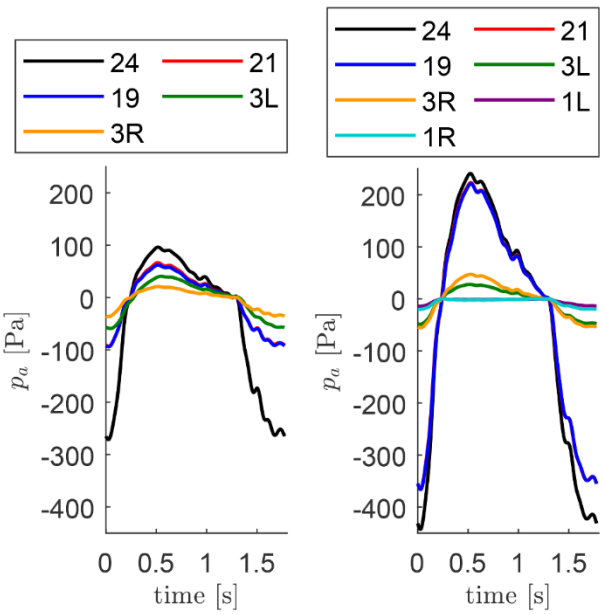

(a) Asymmetric infant (b) Symmetric infant

Fig. 7. Infant models: airway pressure (p_a) as a function of time at various locations (as indicated in Fig. 1a) during non-obstructed respiration without a cannula.

Table 2
Resistance $\Delta p/Q_a$ of the airway between nostrils and trachea (last measurement point) at peak inspiration/expiration of the healthy (adult) and non-obstructed (infants) respiratory profile without NHFT and without cannula, and percentile change due to various cannula sizes (data presented as mean ± standard deviation).

	Cannula	Infant	Symmetric infant	Adult
Peak expiration	none	762 ± 8.9 Pa/(L/s)	1926 ± 13.0 Pa/(L/s)	97 ± 6.4 Pa/(L/s)
	S	68.7 ± 2.2 %	17.6 ± 1.0 %	0.0 ± 11.1 %
	M	75.8 ± 1.9 %	24.7 ± 0.8 %	0.4 ± 8.8 %
	L	135.6 ± 2.6 %	63.2 ± 1.0 %	9.3 ± 10.8 %
Peak inspiration	none	1673 ± 21.8 Pa/(L/s)	2719 ± 17.4 Pa/(L/s)	144 ± 18.2 Pa/(L/s)
	S	32.7 ± 2.7 %	11.6 ± 0.8 %	− 3.6 ± 16.7 %
	M	39.4 ± 2.4 %	16.3 ± 0.9 %	0.5 ± 16.4 %
	L	64.6 ± 2.1 %	47.8 ± 0.9 %	5.8 ± 16.0 %

Resistance is calculated as the mean and standard deviation of the series of resistances evaluated at the inspiration or expiration peaks of the individual respiration cycles.

4.2. Washout

The jet penetration length is an indication for the extent of the washout effect. At end-expiration or end-inspiration, the penetration length is equal to the distance between the prong exits and the location where the pressure becomes uniform: within (adult and symmetric infant) or just after (infant) the nasal cavity. In front of the point where the pressure is uniform, two opposite trends in pressure are observed depending on the specific case: an increase and a decrease towards the constant pressure. The increase is expected from the idea that the NHFT jet reverses and forms an annular return jet, which requires a pressure drop to overcome the resistance of the model. Obviously, the nasal cavity has a complex geometry, and the NHFT jet may flow along the wall instead of through the centre of the channel. Also the formation of vortices is likely due to the turbulent nature of the flow. These fluid mechanical phenomena can explain the decreasing pressure in both nostrils, as observed in the adult model with large cannula.

In the asymmetric infant model, the pressure in the narrow right nostril largely decreases, whereas the pressure in the left nostril increases, and the pressure becomes uniform behind the nasal cavity (where both nostrils merge). This combination may be caused by a 'circulating flow': flow entering one nostril leaves through the other, which is possible when the resistance in one nostril is much larger than the resistance in the nasal cavity and the other nostril. Indeed, the right nostril is clearly smaller than the left nostril, and a large increase in airway resistance was observed with the cannula inserted, which can only be explained by an increased resistance in (the beginning of) the nostril. Also, the symmetric infant shows increasing pressure in both nostrils and has a smaller increase in resistance, indicating that the asymmetry may indeed be of influence.

The observation that the jet reverses in the nasal cavity confirms findings reported by earlier studies. Pressure waveforms were measured in an adult airway model using pressure catheters in the nasopharynx, supraglottis, carina, and test lung [26], which showed that the end-expiratory pressures at these locations were very close. By performing particle image velocimetry (PIV) studies on an adult model, Spence et al. [27,28] demonstrated that the jet reversed early in the nasal cavity, and that the recirculation region increased during inspiration and decreased during expiration. However, visualization studies without respiration showed effective clearance of a tracer gas from the complete nasal cavity [29,30], which seems to be in contradiction with limited jet penetration. Miller et al. [31] performed CFD-simulations to reveal the flow pattern during NHFT for two cannula sizes with open mouth and without respiration, showing that most of the flow left via the mouth.

It is also useful to compare to more fundamental studies on jets in tubes, as one may approximate the complex geometry of the nasal cavity as a circular tube. In congruence to this study, it was found that the jet does not reach the end of long dead-end tubes, but is reversed sooner [32,33]. Interestingly, a simulation study on a confined turbulent axisymmetric jet in counterflow [34] showed that, upon increasing the jet-to-counterflow velocity ratio, the jet penetration length increased to an asymptote of approximately 3.57 times the tube diameter. If a similar limit exists for the irregularly shaped nasal cavity, this would imply that during a respiratory pause the penetration length of the NHFT jet depends neither on the supplied flow rate nor on the cannula size! Indeed, no clear effects were observed from the cannula size on the jet penetration without respiration. In fact, when the nostril area is approximated by a circle, the asymptote of 3.57 times the nostril diameter would give a jet penetration of 52 to 53 mm in the adult model, which is very close to the 55 mm observed in the left nostril. However, further research is needed in which the jet penetration length is determined more accurately, such that the effects from cannula size, cannula positioning, and flow rate can be studied in more detail. Also the effect of high or full occlusion of one nostril (like in the asymmetric infant) might be interesting, as this may cause circulation of the jet instead of reversion in both nostrils.

As expected, the present measurements confirm that NHFT does not provide alveolar washout: there is still considerable dead space between the alveoli and the flushed part of the nasal cavity. The cannula size or flow rate did not seem to have a significant influence on jet penetration and the maximum volume of air that can be cleared. However, a higher flow rate still results in faster clearance of dead space, and can therefore still be beneficial for the washout effect. Despite the remaining dead space, clinical results on gas exchange during NHFT are positive [35].

4.3. Limitations

Obviously, the present study has some limitations. First of all, the number of upper airways is limited: only one adult and one infant geometry were tested. Therefore, the influence of the airway anatomy could not be studied. Although one model suffices to show the order of

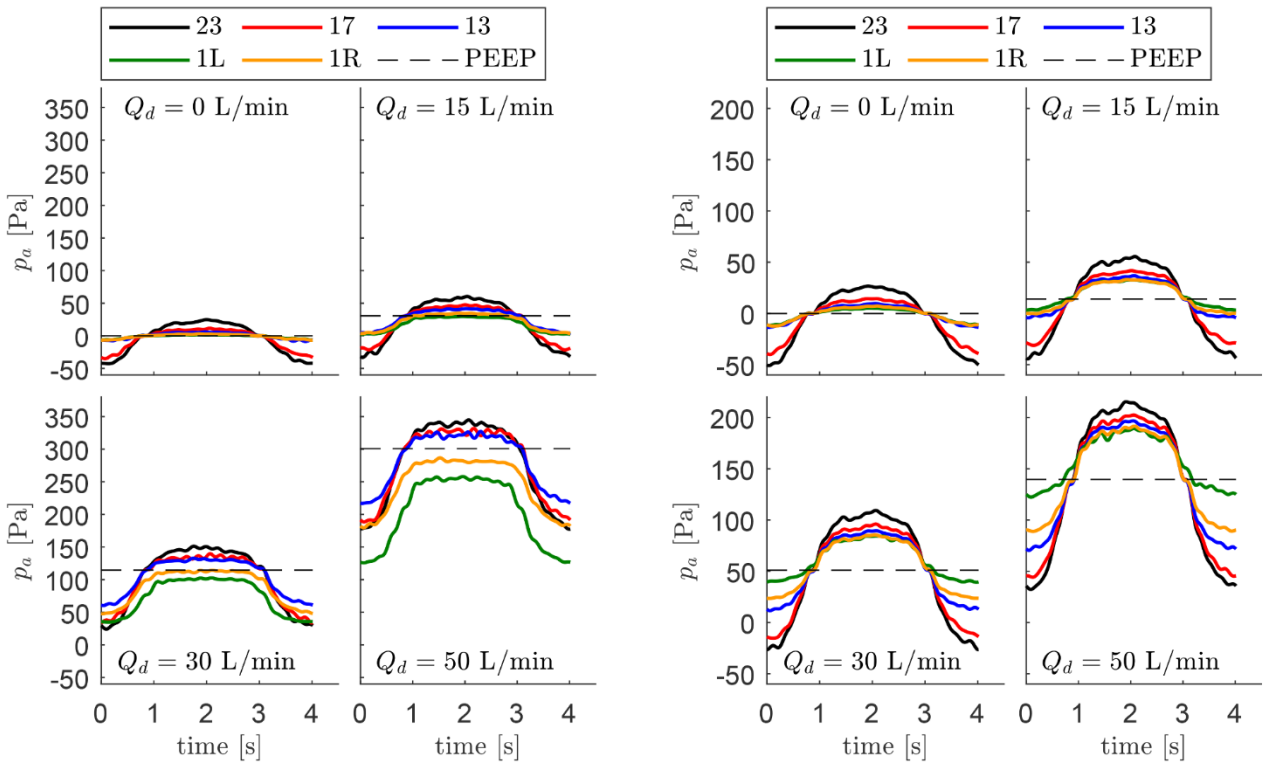

(a) Small cannula (b) Large cannula

Fig. 8. Adult model: airway pressure (p_a) as a function of time during healthy respiration with Nasal High-Flow Therapy at 5 measurement points (as indicated in Fig. 1b).

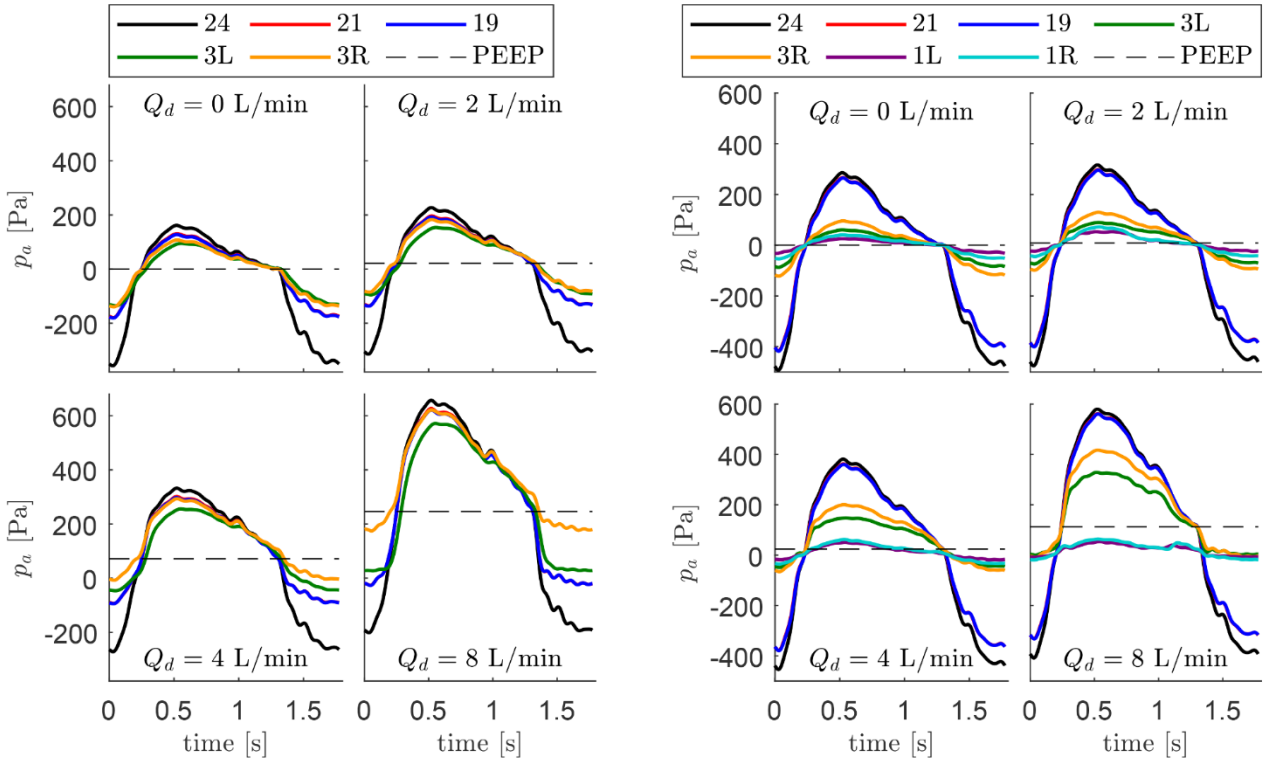

(a) Asymmetric infant model (b) Symmetric infant model

Fig. 9. Infant models: airway pressure (p_a) as a function of time at different measurement points (as indicated in Fig. 1a) during non-obstructed respiration with Nasal High-Flow Therapy using the small cannula.

PEEP-levels and jet penetration lengths, studying more geometries is required to determine numerical relations for clinical practice. Also, it is noted that the symmetric infant model is not representative for any stage in the nasal cycle of congestion and decongestion of the nasal conchae of the asymmetric version. Instead, the symmetric airway should be considered as a different geometry. Although a fully symmetric airway is anatomically unlikely, the aerodynamics are most probably comparable to airways with nearly symmetric nostrils and nasal valves.

Secondly, the upper airway models are rigid and not elastic. Hence, the models are anatomically correct, but the physical features differ from humans.

Thirdly, each cannula was tested at one position only. Positioning was done following the clinical guidelines where possible to mimic a realistic clinical situation. In the infant model, larger insertion lengths of the prongs increase pressures (and vice versa), but quantifying this effect is beyond the scope of this study.

Fourthly, both respiration and NHFT were simulated using cold dry air. Hence, the Reynolds numbers for the mentioned flow rates would be up to 8% lower in the clinical situation with 100% humidity and body temperature. However, from a fluid-mechanical point of view the flow pattern is not significantly affected by this relatively small increment of the Reynolds number, and also the tested Reynolds numbers are relevant for the clinical situations (i.e. the clinical situation with flows that are 8% lower than mentioned is tested).

Finally, when applying NHFT in patients with respiratory distress, the respiration frequency, flow rate, and tidal volume will be higher than in the experiments, and airway resistance may be higher. Consequently, airway pressures during respiration will increase in that case.

5. Conclusion

Working mechanisms of NHFT include the washout of anatomical dead space and provision of PEEP. The extent of both working mechanisms depends on the respiration aerodynamics and the corresponding pressure distribution, but adequate measurements in patients are impossible. The present study presents the pressure distribution along 3D-printed anatomically correct rigid upper airway models of an adult and an infant.

Without respiration, pressure becomes uniform, and the onset of uniform pressure indicates the jet penetration length. The jet penetrates into the nasal cavity of the adult and symmetric infant model, and slightly beyond of the nasal cavity of the symmetric infant model. Consequently, washout is limited to (a part of) the nasal cavity. The jet penetration length hardly depends on cannula size or NHFT flow rate.

The level of uniform pressure equals PEEP. PEEP-levels are low compared to CPAP. PEEP and flow rate are related approximately quadratically: PEEP is roughly doubled when the flow rate is increased by 40%. In the adult model, PEEP is accurately predicted by the dynamic pressure at the prong-exits, but this method fails in the infant models. The relation of PEEP to cannula size depends on the inner and outer diameter of the cannula: a thick-wall cannula would generate most PEEP. For the tested cannulae, PEEP increases with decreasing cannula size for the adult model, whereas the reverse is true for the infant models.

Simulations with respiration and without NHFT showed that the resistance of the cannulae in the adult model was negligible. The resistance is increased more in the symmetric infant model, and most in the asymmetric infant model. The obstruction in the small right nostril of the asymmetric infant model appears to largely influence the resistance, and cannula size may therefore best be determined based on the smallest nostril.

Further research is needed to determine the influences of geometry, cannula insertion length, heating and humidifying, and cannula obstruction.

Funding

This research is financially supported by Longfonds, Fisher & Paykel Healthcare Ltd. and Vivisol Nederland BV, under Longfonds project number 10.1.17.184. The sponsors were not involved in the study design, the collection, analysis and interpretation of data, or the writing or submission of the article.

Ethical approval

Not required.

CRediT authorship contribution statement

Rutger H.J. Hebbink: Conceptualization, Methodology, Software, Validation, Formal analysis, Investigation, Data curation, Writing – original draft, Writing – review & editing, Visualization. **Marieke L. Duiverman:** Writing – review & editing, Supervision, Project administration, Funding acquisition. **Peter J. Wijkstra:** Writing – review & editing, Supervision. **Rob Hagmeijer:** Conceptualization, Methodology, Investigation, Writing – original draft, Writing – review & editing, Supervision, Project administration, Funding acquisition.

Declaration of Competing Interest

The authors have no conflicts of interest to declare.

Acknowledgements

The authors want to acknowledge technician S. Wanrooij of the University of Twente for his large contribution in the design and realisation of the experimental set-up. The authors further acknowledge P. Van Der Meulen of VDM Kunststoftechniek for his advice and efforts in the 3D-printing of the geometries.

Supplementary material

Supplementary material associated with this article can be found, in the online version, at 10.1016/j.medengphy.2022.103805

References

[1] Dysart K, Miller TL, Wolfson MR, Shaffer TH. Research in high flow therapy: Mechanisms of action. Respir Med 2009;103(10):1400–5. https://doi.org/10.1016/j.rmed.2009.04.007.
[2] Finer NN, Mannino FL. High-flow nasal cannula: a kinder, gentler CPAP? J Pediatr. 2009;154(2):160–2. https://doi.org/10.1016/j.jpeds.2008.08.021.
[3] Wilkinson DJ, Andersen CC, Smith K, Holberton J. Pharyngeal pressure with high-flow nasal cannulae in premature infants. J Perinatol 2008;28(1):42–7. https://doi.org/10.1038/sj.jp.7211879.
[4] Liew Z, Fenton AC, Harigopal S, Gopalakaje S, Brodlie M, O'Brien CJ. Physiological effects of high-flow nasal cannula therapy in preterm infants. Arch Dis Child. - Fetal Neonatal Ed 2020;105(1):87–93. https://doi.org/10.1136/archdischild-2018-316773.
[5] Parke RL, Eccleston ML, McGuinness SP. The effects of flow on airway pressure during nasal high-flow oxygen therapy. Respir Care 2011;56(8):1151–5. https://doi.org/10.4187/respcare.01106.
[6] Hasan RA, Habib RH. Effects of flow rate and airleak at the nares and mouth opening on positive distending pressure delivery using commercially available high-flow nasal cannula systems: A lung model study. Pediatr Crit Care Med 2011;12(1):e29–33. https://doi.org/10.1097/PCC.0b013e3181d9076d.
[7] Sivieri EM, Gerdes JS, Abbasi S. Effect of HFNC flow rate, cannula size, and nares diameter on generated airway pressures: An in vitro study. Pediatr Pulmonol 2013;48(5):506–14. https://doi.org/10.1002/ppul.22636.
[8] Nielsen KR, Ellington LE, Gray AJ, Stanberry LI, Smith LS, DiBlasi RM. Effect of high-flow nasal cannula on expiratory pressure and ventilation in infant, pediatric, and adult models. Respir Care 2018;63(2):147–57. https://doi.org/10.4187/respcare.05728.
[9] Wilkins JV, Gardner MT, Walenga R, Hosseini S, Longest PW, Golshahi L. Mechanistic understanding of high flow nasal cannula therapy and pressure support with an in vitro infant model. Ann Biomed Eng 2020;48(2):624–33. https://doi.org/10.1007/s10439-019-02377-z.

[10] Mündel T, Feng S, Tatkov S, Schneider H. Mechanisms of nasal high flow on ventilation during wakefulness and sleep. J Appl Physiol 2013;114(8):1058–65. https://doi.org/10.1152/japplphysiol.01308.2012.
[11] Adams CF, Geoghegan PH, Spence CJ, Jermy MC. Modelling nasal high flow therapy effects on upper airway resistance and resistive work of breathing. Respir Physiol Neurobiol 2018;254:23–9. https://doi.org/10.1016/j.resp.2018.03.014.
[12] Moore CP, Katz IM, Caillibotte G, Finlay WH, Martin AR. Correlation of high flow nasal cannula outlet area with gas clearance and pressure in adult upper airway replicas. Clin Biomech 2019;66:66–73. https://doi.org/10.1016/j.clinbiomech.2017.11.003.
[13] Pinkham M, Tatkov S. Effect of flow and cannula size on generated pressure during nasal high flow. Crit Care 2020;24(1):248. https://doi.org/10.1186/s13054-020-02980-w.
[14] Janssens HM, de Jongste JC, Fokkens WJ, Robben SG, Wouters K, Tiddens HA. The Sophia anatomical infant nose-throat (Saint) model: a valuable tool to study aerosol deposition in infants. J Aerosol Med 2001;14(4):433–41. https://doi.org/10.1089/08942680152744640.
[15] embodi3D.com. Easily Create 3D Printable Muscle and Skin STL Files from Medical CT Scans. https://www.embodi3d.com/blogs/entry/353-easily-create-3d-printable-muscle-and-skin-stl-files-from-medical-ct-scans/; 2016.
[16] Tsilingiris PT. Thermophysical and transport properties of humid air at temperature range between 0 and 100 °C. Energy Convers Manag 2008;49(5):1098–110. https://doi.org/10.1016/j.enconman.2007.09.015.
[17] Borgnakke C, Sonntag RE. Fundamentals of thermodynamics. 8th ed. Hoboken, NJ: Wiley; 2013.
[18] sjfitz. AirProperties. https://github.com/sjfitz/AirProperties; 2021.
[19] Hebbink RHJ, Hagmeijer R. Tidal spirometric curves obtained from a nasal cannula. Med Eng Phys 2021;97:1–9. https://doi.org/10.1016/j.medengphy.2021.09.004.
[20] Mazmanyan P, Darakchyan M, Pinkham MI, Tatkov S. Mechanisms of nasal high flow therapy in newborns. J Appl Physiol 2020;128(4):822–9. https://doi.org/10.1152/japplphysiol.00871.2019.
[21] Van Hove SC, Storey J, Adams C, Dey K, Geoghegan PH, Kabaliuk N, Oldfield SD, Spence CJT, Jermy MC, Suresh V, Cater JE. An experimental and numerical investigation of CO_2 distribution in the upper airways during nasal high flow therapy. Ann Biomed Eng 2016;44(10):3007–19. https://doi.org/10.1007/s10439-016-1604-8.
[22] Nozoe M, Mase K, Murakami S, Okada M, Ogino T, Matsushita K, Takashima S, Yamamoto N, Fukuda Y, Domen K. Relationship between spontaneous expiratory flow-volume curve pattern and air-flow obstruction in elderly COPD patients. Respir Care 2013;58(10):1643–8. https://doi.org/10.4187/respcare.02296.
[23] Hevroni A, Goldman A, Blank-Brachfeld M, Ahmad WA, Ben-Dov L, Springer C. Use of tidal breathing curves for evaluating expiratory airway obstruction in infants. J Asthma 2018;55(12):1331–7. https://doi.org/10.1080/02770903.2017.1414234.
[24] Nishimura M. High-flow nasal cannula oxygen therapy in adults. J Intensive Care 2015;3(1):15. https://doi.org/10.1186/s40560-015-0084-5.
[25] Kushida C, Chediak A, Berry R, Brown L, Gozal D, Iber C, Parthasarathy S, Quan S, Rowley J. Clinical guidelines for the manual titration of positive airway pressure in patients with obstructive sleep apnea. J Clin Sleep Med 2008;4(2):157–71. https://doi.org/10.5664/jcsm.27133.
[26] Luo J-c, Lu M-s, Zhao Z-h, Jiang W, Xu B, Weng L, Li T, Du B. Positive end-expiratory pressure effect of 3 high-flow nasal cannula devices. Respir Care 2017;62(7):888–95. https://doi.org/10.4187/respcare.05337.
[27] Spence CJT, Buchmann NA, Jermy MC, Moore SM. Stereoscopic PIV measurements of flow in the nasal cavity with high flow therapy. Exp Fluids 2011;50(4):1005–17. https://doi.org/10.1007/s00348-010-0984-z.
[28] Spence CJT, Buchmann NA, Jermy MC. Unsteady flow in the nasal cavity with high flow therapy measured by stereoscopic PIV. Exp Fluids 2012;52(3):569–79. https://doi.org/10.1007/s00348-011-1044-z.
[29] Möller W, Celik G, Feng S, Bartenstein P, Meyer G, Eickelberg O, Schmid O, Tatkov S. Nasal high flow clears anatomical dead space in upper airway models. J Appl Physiol 2015;118(12):1525–32. https://doi.org/10.1152/japplphysiol.00934.2014.
[30] Möller W, Feng S, Domanski U, Franke K-J, Celik G, Bartenstein P, Becker S, Meyer G, Schmid O, Eickelberg O, Tatkov S, Nilius G. Nasal high flow reduces dead space. J Appl Physiol 2016;122(1):191–7. https://doi.org/10.1152/japplphysiol.00584.2016.
[31] Miller TL, Saberi B, Saberi S. Computational fluid dynamics modeling of extrathoracic airway flush: evaluation of high flow nasal cannula design elements. Pulm Respir Med 2016;6(5):1–7. https://doi.org/10.4172/2161-105X.1000376.
[32] Amano RS. A numerical study of turbulent axisymmetric jets flowing into closed tubes. J Energy Resour Technol 1986;108(4):286–91. https://doi.org/10.1115/1.3231278.
[33] Crane J, Neumeier Y, Bhave P, Zinn B. Approximate solution of a laminar jet discharged into a dead end tube. 47th AIAA aerospace sciences meeting including the new horizons forum and aerospace exposition, aerospace sciences meetings. Orlando, Florida: American Institute of Aeronautics and Astronautics; 2009. https://doi.org/10.2514/6.2009-387.
[34] Sivapragasam M, Deshpande MD, Ramamurthy S, White P. Turbulent jet in confined counterflow. Sadhana 2014;39(3):713–29. https://doi.org/10.1007/s12046-013-0225-2.
[35] Bräunlich J, Mauersberger F, Wirtz H. Effectiveness of nasal highflow in hypercapnic COPD patients is flow and leakage dependent. BMC Pulm Med 2018;18(1):14. https://doi.org/10.1186/s12890-018-0576-x.